

# Electron-phonon interaction and superconductivity in metallic molecular hydrogen.

## II. Superconductivity under pressure

P. Cudazzo,<sup>1</sup> G. Profeta,<sup>1</sup> A. Sanna,<sup>2,3,4</sup> A. Floris,<sup>3,4</sup> A. Continenza,<sup>1</sup> S. Massidda,<sup>2</sup> and E. K. U. Gross<sup>3,4</sup>

<sup>1</sup>*CNISM-Dipartimento di Fisica, Università degli Studi dell'Aquila, Via Vetoio 10, Coppito, I-67010 L'Aquila, Italy*

<sup>2</sup>*CNR-IOM-SLACS and Dipartimento di Fisica, Università di Cagliari, I-09124 Monserrato, Cagliari, Italy*

<sup>3</sup>*Institut für Theoretische Physik, Freie Universität Berlin, Arnimallee 14, D-14195 Berlin, Germany*

<sup>4</sup>*European Theoretical Spectroscopy Facility (ETSF)*

(Received 7 January 2010; published 2 April 2010)

A detailed study of the electron-phonon interaction in the *Cmca* phase of metallic hydrogen and of its implications in the superconducting properties is presented. A careful analysis of the role played by anisotropy and by the presence of superconducting multigaps allows to single out the peculiarities that drive superconductivity at very high temperature in this system.

DOI: [10.1103/PhysRevB.81.134506](https://doi.org/10.1103/PhysRevB.81.134506)

PACS number(s): 74.62.Fj, 74.20.Pq, 74.25.Jb, 74.25.Kc

### I. INTRODUCTION

The anisotropic and multiband nature of electron-phonon (el-ph) coupling in materials leads to the appearance of many interesting phenomena, only recently partially investigated thanks to the improved resolution of the experimental techniques. One of the most striking examples was the discovery of two-band superconductivity in  $\text{MgB}_2$  (Ref. 1) which opened new theoretical questions on the interplay of anisotropy and multiband of the electron-phonon coupling. The first and most important consequence is the enhanced superconducting (SC) critical temperature of 39 K, about doubled in comparison to the predicted single band isotropic value. Some other recent discoveries of multiband (mostly two-band) superconductivity and gap anisotropies were reported for calcium intercalated graphite ( $\text{CaC}_6$ ),<sup>2</sup> borocarbides ( $\text{YNi}_2\text{B}_2\text{C}$ ),<sup>3</sup> iron silicides,<sup>4</sup> dicalcogenides,<sup>5</sup> and on the recently discovered iron pnictides superconductors.<sup>6-8</sup>

In order to correctly describe, by means of computational techniques, the physical consequences of multiband superconductivity on the critical temperature it is of fundamental importance to account for the  $k$  and band anisotropy. This last point was recently discussed in a fully anisotropic calculation on dense molecular hydrogen,<sup>9</sup> based on the SC density-functional theory (SCDFT):<sup>10-12</sup> there, the occurrence of *three*-band superconductivity was reported.<sup>9</sup> A detailed study of the structural, electronic, and dynamical properties of this particular molecular metallic phase is presented in Ref. 13; here, we present an exhaustive description of the electron-phonon coupling strength in dense molecular hydrogen and how it leads to the prediction of three-gaps superconductivity. In particular, we will show how this unusual superconducting phase is a direct consequence of: (i) the different nature of the electronic states at the Fermi level ( $E_F$ ); (ii) the rich Fermi-surface (FS) topology, and (iii) the different electron-phonon coupling strength with particular phonon branches.

The paper is organized as follows: we will give some details regarding the computational method and the parameters used in the calculation in Sec. II. Then, we will focus on the el-ph interaction, analyzing in its intraband and interband contributions, and on how it is affected by pressure

(Sec. III) and on the superconducting properties (Sec. IV). Finally, we will draw our conclusions in Sec. V.

### II. COMPUTATIONAL DETAILS

The study of the SC phase of hydrogen is performed according to the formalism of SCDFT.<sup>10-12</sup> We considered the *Cmca* phase, a molecular metallic phase with two  $\text{H}_2$  molecules per unit cell stacked along different planes.<sup>9,13</sup> The SC properties are calculated solving a generalized gap equation including both attractive el-ph interaction and repulsive electron-electron effective interaction. Both the interactions are treated in a fully anisotropic formalism, allowing wave vector ( $\mathbf{k}$ ) and band ( $n$ ) anisotropy (isotropic approximations are used only when clearly stated). We computed the el-ph matrix elements  $|g_{n\mathbf{k},n'\mathbf{k}+\mathbf{q}}^\nu|^2$ , for each phonon mode  $\nu$ , on a regular mesh of  $6^3$   $\mathbf{q}$  points and  $16^3$   $\mathbf{k}$  points, while the Coulomb matrix elements have been calculated on  $9^3 \times 9^3$   $\mathbf{k}$  and  $\mathbf{k}'$  points. As well known, the SC gap is a function extremely peaked around the Fermi surface, while at higher energies it is rather smooth. This implies that a converged solution of the gap equation needs a denser  $\mathbf{k}$ -points sampling around  $E_F$  and a coarser one elsewhere. This nonuniform mesh in the irreducible Brillouin zone (IBZ) is realized using  $6 \times 10^3$  (800) independent  $\mathbf{k}$  points for bands crossing (not crossing)  $E_F$ . The latter choice ensures a convergence within 2% on the  $T_c$  value. The study of the el-ph coupling has been performed through the calculation of the Eliashberg function  $\alpha^2F(\omega)$  and of the el-ph coupling constant  $\lambda$ , whose expressions read:

$$\alpha^2F(\omega) = \frac{1}{N(E_F)} \sum_{nn'} \sum_{\mathbf{k}, \mathbf{q}\nu} |g_{n\mathbf{k},n'\mathbf{k}+\mathbf{q}}^\nu|^2 \times \delta(\epsilon_{n\mathbf{k}}) \delta(\epsilon_{n'\mathbf{k}+\mathbf{q}}) \delta(\omega - \omega_{\nu\mathbf{q}}),$$

$$\lambda = 2 \int \frac{\alpha^2F(\omega)}{\omega} d\omega,$$

where  $N(E_F)$  is the density of states (DOS) at  $E_F$ , taken as the zero of the energy scale. In  $\alpha^2F(\omega)$ , the double integral

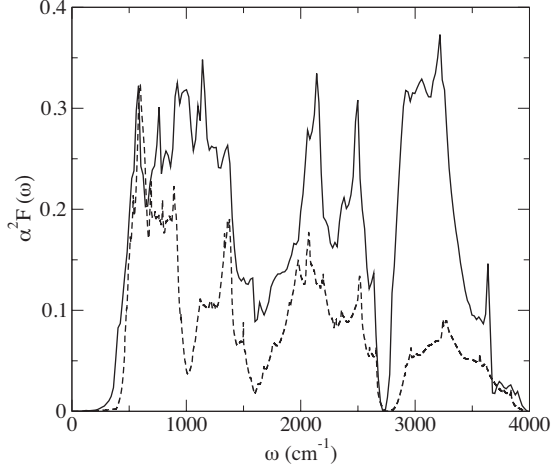


FIG. 1.  $\alpha^2 F(\omega)$  function of hydrogen at 414 GPa (solid line) compared with the rescaled (to align the heights of the first peak density of states) (dashed line).

on the FS involving the electron eigenvalues  $\epsilon_{n\mathbf{k}}$  and  $\epsilon_{n'\mathbf{k}+\mathbf{q}}$  has been calculated using the same method to integrate the gap equation, that is, integrating over  $6 \times 10^3$   $\mathbf{k}$  points on FS. This allows to obtain a convergence of about 2% on the  $\lambda$  value.

### III. ELECTRON-PHONON INTERACTION

The analysis of the dynamical properties of H under pressure<sup>13</sup> showed a rich and interesting phonon spectrum. In particular, the presence of many phonon softenings<sup>13</sup> along the  $k_x$  and  $k_y$  directions of the IBZ, can be a signature of strong el-ph coupling. The analysis suggests a strong renormalization for vibron and libron  $A_g$  modes near  $\Gamma$  and for the acousticlike phonon mode  $B_{2u}$ , libron  $B_{3g}$ , and vibron modes at larger wave vectors. A signature of strong el-ph coupling could be searched in the behavior of the phonon linewidths  $\gamma_{\nu,\mathbf{q}}$ .

In agreement with calculations of Zhang *et al.*,<sup>14</sup> this quantity reveals a large peak close to the  $\Gamma$  point at the libronic and vibronic  $A_g$  modes, the most strongly coupled phonons. However, along the  $k_x$  direction,  $\gamma_{\nu,\mathbf{q}}$  does not indicate strong el-ph interaction for the  $B_{3g}$  libron mode or the  $B_{2u}$  acoustic mode, suggesting that the softening on these modes at the nesting vectors  $\mathbf{q}=(0.47\frac{2\pi}{a}, 0, 0)$  (Ref. 15) are pure Kohn anomalies, meaning by this that they are related only to the FS topology, and not to particularly strong el-ph matrix elements. Along the  $k_z$  direction the el-ph coupling is weak in comparison to other in-plane directions: in fact, no phonon renormalizations appear along the  $\Gamma$ -Z line.<sup>13</sup>

Further understanding of the coupling is gained by examining the  $\alpha^2 F(\omega)$  Eliashberg function, showed in Fig. 1 at  $P=414$  GPa and compared with the phonon density of states. Both plots are characterized by three frequency regions: in the first region,  $\omega \leq 1600$   $\text{cm}^{-1}$ , the larger contribution to the el-ph coupling is due to the libron mode ( $A_g$ ) near  $\Gamma$  and to the opticlike and acousticlike phonon modes at large  $\mathbf{q}$ . In the second region ( $1600 \leq \omega \leq 2700$   $\text{cm}^{-1}$ ), the main contributions come from the in-phase and out-of-phase

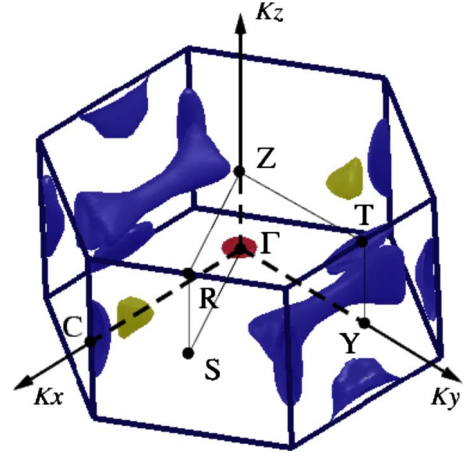


FIG. 2. (Color online) Electron-phonon coupling constant at 414 GPa. Different colors label different values of  $\lambda_{\mathbf{k}}$  projected on the Fermi surface. Disk at  $\Gamma$ -point ( $1.80 < \lambda_{\mathbf{k}} < 2.00$ ), light gray ( $1.00 < \lambda_{\mathbf{k}} < 1.80$ ), and the other sheets ( $\lambda_{\mathbf{k}} < 1.00$ ). These regions will be referred to as R1, R2, and R3 in the text.

libron modes in the  $k_{yz}$  plane and the phononic modes along the  $k_z$  axis at large wave vectors. A comparison between the spectral function and the phonon density of states (not shown) shows that the peaks at  $\omega=2000$   $\text{cm}^{-1}$  and  $\omega=2500$   $\text{cm}^{-1}$  are essentially due to the large values of the phonon DOS while the region at around  $1000$   $\text{cm}^{-1}$  (corresponding to the  $A_g$  libronic mode at  $\Gamma$ ) is characterized by a strong el-ph coupling and a minimum in the phonon DOS. Finally, the high-frequency region reveals a strong coupling of the vibron modes.

Turning to the band-resolved el-ph coupling, we classify the energy bands as  $\epsilon_{nn'}$ : here the indices  $n, n'=b, a$  define bonding and antibonding combinations, and their position as first and second index marks the intramolecular and intermolecular character, respectively (see also Ref. 13). The band-resolved el-ph coupling constants  $\lambda_{n\mathbf{k}}$  at the Fermi surface are calculated according to,

$$\lambda_{n\mathbf{k}} = 2 \sum_{n'\mathbf{k}',\nu} \frac{|g_{\mathbf{k},\mathbf{k}',\nu}^{nn'}|^2}{\omega_{\mathbf{k}'-\mathbf{k},\nu}} \times \delta(\epsilon_{n'\mathbf{k}'}). \quad (1)$$

Figure 2 shows the Fermi surface colored according to the  $\lambda_{n\mathbf{k}}$  values of each band: the strong dependence of the el-ph coupling on the band index as well as the enhanced anisotropy in  $\mathbf{k}$  space are clearly evidenced. In particular, three FS regions can be easily recognized with rather different el-ph coupling: the largest coupling occurs at the disk surrounding  $\Gamma$  (originating from the  $\epsilon_{ab}$  band); intermediate el-ph coupling values characterize the two prismlike structures on the  $xy$  plane belonging to the  $\epsilon_{ba}$  band and the other sheets from the  $\epsilon_{ba}$ ,  $\epsilon_{ab}$ , and  $\epsilon_{aa}$  bands; the region showing the smallest  $\lambda_{\mathbf{k}}$  is the tubular sheet coming from the  $\epsilon_{ba}$  band.

The peculiar nature of the charge distribution (bonding nature) in this system is the cause of a strongly anisotropic el-ph coupling and, as we shall see, of multigap superconductivity. This particular distribution of  $\lambda_{n\mathbf{k}}$  over the FS allows in fact a multiband description of  $\alpha^2 F(\omega)$  in which the

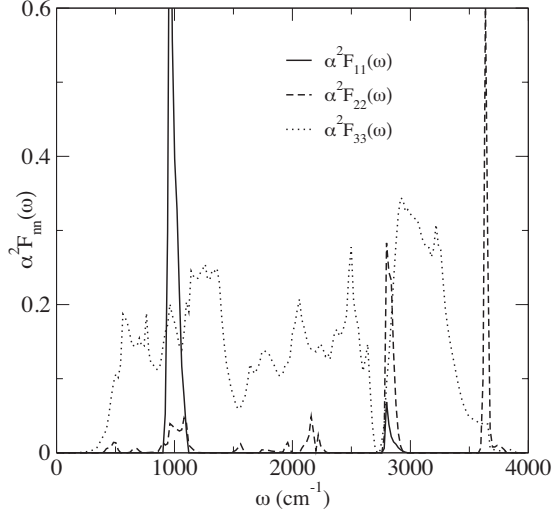


FIG. 3. Intraband contribution to the spectral function for  $R_1$ ,  $R_2$ , and  $R_3$  regions.

integration over the FS is separated in three contributions related to the three regions ( $R_1$ ,  $R_2$ , and  $R_3$ ) corresponding to different el-ph coupling, as shown in Fig. 2: (i)  $R_1$ : the disk at  $\Gamma$  arising from the band  $\epsilon_{ba}$ ; (ii)  $R_2$ : the two prislake structures belonging to the band  $\epsilon_{ba}$ ; (iii)  $R_3$ : the tubular structures of the  $\epsilon_{ba}$  band and all the remaining FS portions.

Accordingly, we can define a partial Eliashberg function  $\alpha^2 F_{nn'}(\omega)$  for each region  $R_n$  ( $n=1,2,3$ ) as follows:

$$\alpha^2 F_{nn'}(\omega) = \frac{1}{N_n(0)} \sum_{\mathbf{k} \in R_n} \sum_{\mathbf{k}' \in R_{n'}} \sum_{\nu} |g_{n\mathbf{k},n'\mathbf{k}'}^{\nu}|^2 \times \delta(\epsilon_{n\mathbf{k}}) \delta(\epsilon_{n'\mathbf{k}'}) \delta(\omega - \omega_{\nu\mathbf{k}'-\mathbf{k}}) \quad (2)$$

with the corresponding partial matrix elements  $\lambda_{nn'}$ ,

$$\lambda_{nn'} = 2 \int \frac{\alpha^2 F_{nn'}(\omega)}{\omega} d\omega. \quad (3)$$

### A. Intraband and interband electron-phonon couplings

We first analyze the intraband contributions. Figure 3 shows  $\alpha^2 F_{nn}(\omega)$  for the three different FS regions previously defined: the main features come from region  $R_1$  in  $\alpha^2 F_{11}(\omega)$  at about  $1000 \text{ cm}^{-1}$  (the libron mode  $A_g$  in the  $yz$  plane at  $\Gamma$ ) and  $R_2$ , with two peaks in  $\alpha^2 F_{22}(\omega)$  at  $\omega=2800 \text{ cm}^{-1}$  ( $A_g$  in phase vibron at  $\Gamma$ ) and at  $\omega=3640 \text{ cm}^{-1}$  due to the nesting  $\mathbf{q}$ -wave vector connecting the prislake regions.

A direct and clear understanding of the large coupling of the  $A_g$  libron and vibron modes at  $\Gamma$  ( $\omega=1000 \text{ cm}^{-1}$  and  $2800 \text{ cm}^{-1}$ , respectively) can be obtained looking at the effects of the related normal mode displacements on the electronic wave functions at the Fermi level. Deformations along the libron mode bring H atoms belonging to different planes closer, thus increasing the overlap between neighboring in-layer  $\psi_{ba}(\mathbf{r})$  states and, at the same time, reducing superposition among interlayer  $\psi_{ab}(\mathbf{r})$  states (see Ref. 13, Fig. 5). On the other hand, the vibronic mode, being an intramolecular

TABLE I. Intraband el-ph coupling calculated according to the Kahn-Allen scheme compared with the same quantities calculated from the partial Eliashberg functions.

FS region	$\lambda_{A_g^l}$	$\lambda_{B_{3g}}$	$\lambda_{A_g^v}$	$2 \int \frac{\alpha^2 F(\omega)}{\omega}$
$R_1$	0.12			0.14
$R_2$			0.02	0.05
$R_3(\epsilon_{ba})$	0.13		0.03	0.28
$R_3(\epsilon_{ab})$	0.06	0.03	0.01	0.26
$R_3(\epsilon_{aa})$		0.01	0.01	0.03

bond-stretching mode, favors charge transfer between intramolecular and intermolecular regions (i.e., from  $\epsilon_{ba}$  toward  $\epsilon_{aa}$  states) and increases the overlap among states localized on adjacent layers.

The feature at higher frequency in  $\alpha^2 F_{22}(\omega)$  ( $\omega=3640 \text{ cm}^{-1}$ ) is due to intraband scattering processes among prislake structures and thus is related to intralayer charge modulation within the  $\psi_{ba}(\mathbf{r})$  wave function on the  $R_2$  region. The situation for the intraband coupling within the  $R_3$  region is more complex: here, unlike for the previous FS sheets, it is not possible to attribute the el-ph coupling to a single phonon mode since the partial  $\alpha^2 F_{33}(\omega)$  extends all over the phonon spectrum. This is partially due to the presence of many different  $\mathbf{q}$ 's connecting the various sheets of region  $R_3$ .

To give a quantitative evaluation of the role played by the libron and vibron modes at low wave vectors in the intraband scattering, we compare the matrix elements calculated from Eq. (3), with the partial el-ph coupling of these phonon modes obtained according to the Kahn and Allen approach.<sup>16</sup> In the latter, the intraband el-ph coupling constants are calculated in terms of deformation potential,

$$\lambda_{nn} = N_n \frac{\hbar^2}{2M\omega^2} \left| \sum_a D_a \right|^2, \quad (4)$$

here, the sum over  $a$  runs over the four moving H atoms in the unit cell,  $N_n$  is the partial density of states at  $E_F$  per spin in region  $R_n$ ,  $D_a$  is the deformation potential mean value in  $R_n$ , and  $\omega$  is the phonon frequency.

We can therefore calculate the energy variation in each band crossing  $E_F$  upon atomic displacements along eigenvectors relative to: the libron mode  $A_g^l$ , the in-phase  $A_g^v$  and the out-of-phase  $B_{3g}$  vibron modes (the superscript  $l$  and  $v$  referring to libron and vibron, respectively). Our results for the  $\lambda$  values are summarized in Table I.

Comparing these values of  $\lambda$  with those obtained integrating the partial Eliashberg function as in Eq. (3) (last column of Table I), it is evident that the entire contribution to the el-ph coupling within the disk  $R_1$  arises from the libron mode at  $\Gamma$  while the two prislake structures ( $R_2$ ) and the region  $R_3$  belonging to the band  $\epsilon_{aa}$  have their main contributions from the vibron mode at  $\Gamma$ .

Interband scattering provides an additional possible channel for el-ph scattering which could turn out to be very efficient: in fact, if the number and the area of Fermi surfaces,

formed by  $\mathbf{q}$  vectors satisfying the nesting condition, is large enough, then the interband scattering can be substantial even if the corresponding matrix elements are not particularly large. We find that the main contribution to the interband Eliashberg function arises from scattering among bonding ( $R_2$ , and part of  $R_3$ ) and antibonding ( $R_1$ ) states.

We conclude this section calculating from Eq. (3) the  $\lambda_{nm'}$  matrix elements of the  $\bar{\lambda}$  matrix and the effective electronic interaction potential matrix  $\bar{V}$  for all the regions at  $E_F$ . The matrix elements  $V_{nm'}$  of the  $\bar{V}$  matrix represent the effective interaction mediated by phonons within a BCS scheme and are defined as:  $N_{n'}V_{nm'} = \lambda_{nm'}$ ,  $N_{n'}$  being the density of states of band  $n'$  at  $E_F$ . The matrix elements describe the scattering amplitude for two electrons in band  $n$  to scatter to band  $n'$  exchanging a phonon. The results for both matrix elements read,

$$\bar{\lambda} = \begin{pmatrix} 0.14 & 0.37 & 1.44 \\ 0.20 & 0.05 & 0.82 \\ 0.11 & 0.11 & 0.70 \end{pmatrix}, \quad (5)$$

$$\bar{V}(Ry) = \begin{pmatrix} 4.32 & 6.00 & 3.18 \\ 6.00 & 0.90 & 1.82 \\ 3.18 & 1.82 & 1.56 \end{pmatrix}. \quad (6)$$

We note how the small density of states  $N_1$  results in lower intraband value for  $\lambda_{11}$  with respect to  $\lambda_{33}$ , despite the much larger intraband matrix element  $V_{11}$  between  $R_1$  states. Finally, we point out the case of the large intraband  $\alpha^2F_{22}$  contribution resulting, however, in a rather small  $V_{22}$  term: here, the high frequency of the coupled vibron strongly renormalizes the el-ph matrix element.

### B. Effect of pressure

In this section we discuss how the el-ph coupling changes with pressure. It is well known that applied pressure on a molecular system determines a delocalization of the wave functions which in turn results in two main competing effects on the el-ph interaction: (i) it increases the bare el-ph matrix elements due to the larger overlap between wave functions from different sites; (ii) it increases the electronic screening of the phonon deformations; (iii) additional effects could be related to possible changes in FS structure, such as formation of new branches at  $E_F$  or variations in the nesting of Fermi surface portions.

In Fig. 4 the Eliashberg function at  $P=414$  and  $462$  GPa is shown: increased pressure strongly enhances the coupling all over the phononic spectra through several mechanisms: (i) it raises the DOS at  $E_F$  (see Fig. 7 of Ref. 13); (ii) it makes the el-ph coupling stronger; (iii) it increases the FS available bringing two bands ( $\epsilon_{ab}$  and  $\epsilon_{aa}$ ) below  $E_F$  near the  $R$  point of the IBZ (see Fig. 6 of Ref. 13), thus generating a new channel for el-ph interaction. The latter is responsible for the abrupt change in  $\lambda$  at pressures between  $P=425$  and  $440$  GPa (Fig. 5) and originates eight new FS structures at  $z = \pm \frac{\pi}{c}$  (see Fig. 8 of Ref. 13) characterized by two new branches  $R_4$  and  $R_5$ , respectively. The intraband scattering in

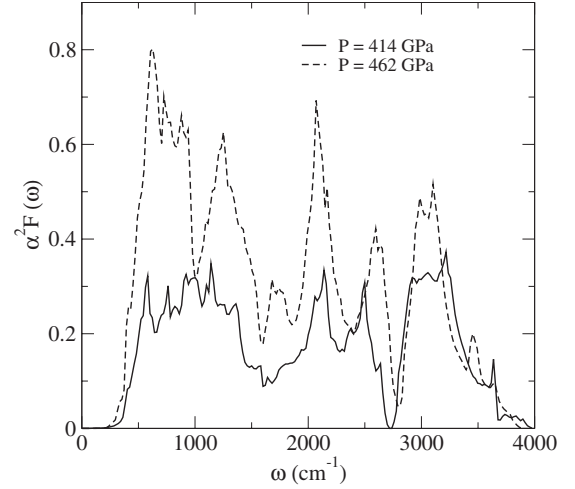


FIG. 4.  $\alpha^2F(\omega)$  at 414 GPa (solid line) and 462 GPa (dashed line).

these sheets arises from the  $B_{3g}$  libron mode in the  $yz$  plane at  $\Gamma$  and at the wave vectors connecting different sheets of  $R_4$  and  $R_5$  on the same plane. We notice (Fig. 4 of Ref. 13) that the bands  $\epsilon_{ab}$  and  $\epsilon_{aa}$  are degenerate at the  $R$  point; the activation of the  $B_{3g}$  libron removes the energy degeneracy inducing charge transfer from  $\epsilon_{ab}$  to  $\epsilon_{aa}$  and therefore a strong el-ph coupling (libron  $B_{3g}$ ). Its signature on the total  $\alpha^2F(\omega)$  is the new feature at around  $1750 \text{ cm}^{-1}$  (Fig. 4). A very large contribution to the overall el-ph coupling on these new regions comes from interband el-ph scattering with  $R_2$  and  $R_3$ , involving low-frequencies phononic modes at large wave vectors.

The role played by these new sheets in the el-ph coupling can be investigated comparing the el-ph coupling constant evaluated with ( $\lambda$ ) and without ( $\lambda'$ ) contributions coming from regions  $R_4, R_5$ . The results shown in Fig. 5 indicate that these regions contribute over 40% the value of the total  $\lambda$ , despite the rather low density of states associated to the corresponding FS sheets.

To better point out the effect of the density of states at  $E_F$  we also show in Fig. 5 the behavior of  $V = \frac{\lambda}{N(\epsilon_F)}$ . In the high-

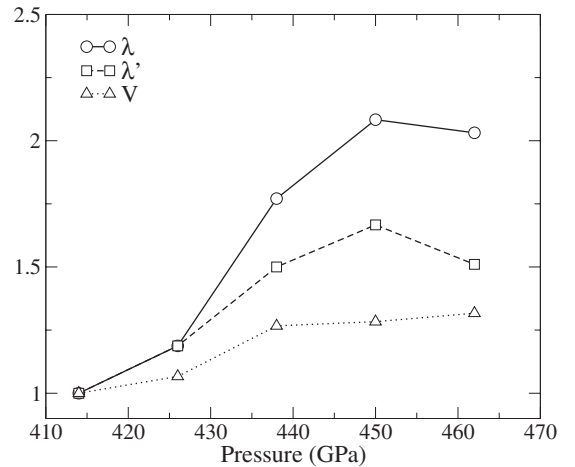


FIG. 5. Behavior of the el-ph coupling calculated in different approximation (see text) as a function of pressure. All the values plotted are scaled to their respective values at  $P=414$  GPa.

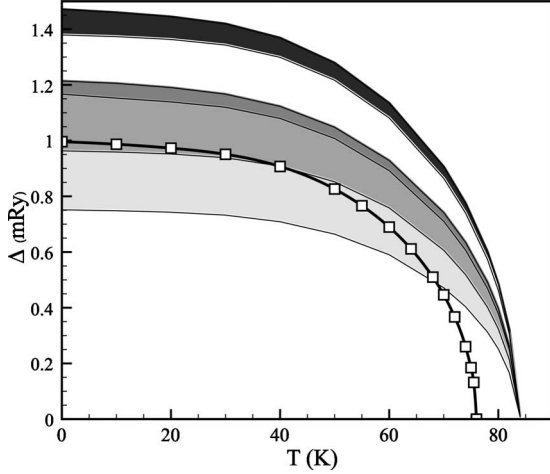


FIG. 6. Isotropic (squares) and anisotropic  $\Delta_{nk}$  (with  $\mathbf{k}=k_F$ ) at  $E_F$  at  $P=414$  GPa. The shaded regions represent the  $k$  anisotropy over different bands (note the overlapping gaps between 13.00 and 15.75 meV).

pressure regime,  $V$  (i.e., the mean value of el-ph matrix elements) shows only a slight enhancement at high pressure indicating that it is the increased DOS that dominates the  $\lambda$  behavior: the lower value of  $\lambda$  at 462 GPa is, in fact, due to a small reduction in the DOS at  $E_F$  with respect to its value at 450 GPa.

#### IV. SUPERCONDUCTING PHASE

The superconducting phase of molecular metallic hydrogen has been investigated solving the SCDFC gap equation. Band and  $\mathbf{k}$ -anisotropy contributions can be singled out solving the gap equation in two cases: (i) taking into account the full  $(n, \mathbf{k})$  dependency of the el-ph and Coulomb matrix elements and (ii) including only their average on the Fermi surface (isotropic approximation).

##### A. Isotropic approximation

We start our discussion considering the isotropic approximation: here, the el-ph interaction is included via the Eliashberg function and the Coulomb interaction is treated assuming a screening within the Sham-Kohn<sup>17</sup> approach and using plane-waves wave functions rather than crystal Bloch functions.

Figure 6 (empty squares) shows the energy gap at  $E_F$ , as a function of temperature at  $P=414$  GPa, obtained solving self-consistently the SCDFC gap equation in the isotropic approximation. The critical temperature obtained for a vanishing gap value is  $T_c=76$  K. Due to the strong el-ph coupling present in this system, the ratio  $\frac{2\Delta}{k_B T_c}$  is about 4.15, quite larger than the value (3.53) predicted by the BCS theory. As a function of pressure (see Fig. 8, dashed line) the critical temperature follows the behavior of  $\lambda$  (cf. Figure 5): it increases from 76 to 226 K at  $P=450$  GPa, then decreases to 219 K at  $P=462$  GPa, once again following the  $\lambda$  behavior.

TABLE II. Superconducting gap and critical temperature in the multigap BCS approximation and SCDFC.

	$\Delta_1/\Delta_3$	$\Delta_2/\Delta_3$	$\Delta_3/\Delta_3$	$\frac{T_c - T_c^{iso}}{T_c} \times 100$ (%)
BCS multigap	1.48	1.11	1.00	9.4
SCDFC	1.42	1.13	1.00	10

##### B. Anisotropy and multigap superconductivity

The anisotropic SC gaps at  $E_F$  at  $P=414$  GPa, including the screened Coulomb interaction within random-phase approximation (RPA), are shown on Fig. 6 (shaded regions). As inferred from the previous analysis of the el-ph interaction, hydrogen is expected to show multigap superconductivity. In fact, three gaps are easily distinguishable, their energy width being related to  $\mathbf{k}$ -space anisotropy: a largest one (19.3 meV at  $T=0$ ), and two very anisotropic, overlapping gaps. As anticipated, the three gaps are associated to different FS sheets: the strongly coupled disk around the  $\Gamma$  point ( $R_1$ , larger gap), the “prismlike” sheets ( $R_2$ , intermediate gap), and the remaining FS portions ( $R_3$ ) associated with the lowest gap.

A model picture for superconductivity in  $H_2$  under pressure, within a BCS framework, can now be derived. Starting from our general gap equation, using the defined partial Eliashberg functions and including Coulomb interactions through the  $\bar{\mu}$  matrix (rather than  $\mu^*$ , due to the weak renormalization), taking the limits  $\varepsilon, \varepsilon' \rightarrow 0$ , and  $\beta \rightarrow \infty$  to evaluate the kernels,<sup>15</sup> it is possible to derive the following BCS-type expression for the gaps,

$$\Delta_n = \frac{1}{2 \left( 1 + \sum_{n'} \lambda_{nn'} \right)} \sum_{n'} (\lambda_{nn'} - \mu_{nn'}) \times \int dE' \frac{\tanh\left(\frac{\beta}{2} E'\right)}{E'} \Delta_{n'}.$$

This equation can be casted in an eigenvalue problem and solved for the eigenvectors  $\Delta_n$ , as reported in Table II.

It is interesting to observe that model-BCS qualitatively reproduces the SCDFC gaps, while the isotropic approximation, as usual, underestimates  $T_c$ . Now a question arises: how does the presence of several gaps concur together with  $\mathbf{k}$  anisotropy to enhance the transition temperature? We should distinguish two different limits: (i) large and (ii) small values of the off-diagonal terms in the kernel matrix. In the first case, interband coupling is comparable or even larger than intraband coupling, resulting in Cooper pairs delocalized over the entire FS: thus, a more isotropiclike behavior should be reasonably expected (i.e.,  $T_c \simeq T_c^{iso}$ ). Large values of the off-diagonal matrix elements, in fact, would destroy the effect of anisotropy and result in a modest enhancement of  $T_c$ . In the second case, i.e., small values of interband coupling, the Cooper pairs are very localized within their own band and an isotropic treatment should not be satisfactory. In the limit of vanishing interband coupling, in fact, multiband ef-

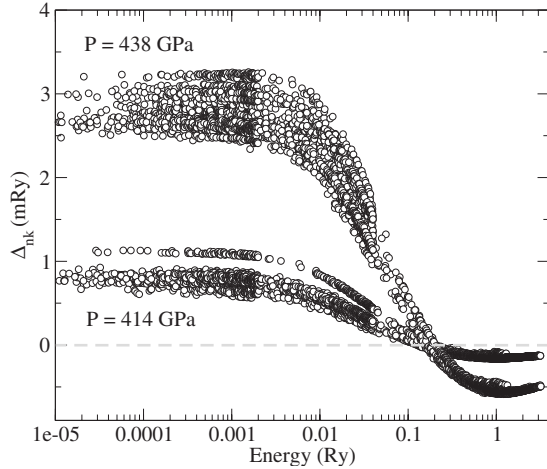


FIG. 7. Behavior of the anisotropic gaps at  $T=0$  K as a function of (positive) energy distance from  $E_F$  at  $P=414$  and  $P=438$  GPa.

fects can enhance superconductivity since  $T_c$  is related to the larger eigenvalue of the kernel matrix, i.e., to the larger intraband effective interaction. In this case, multiband contributions can have dramatic effects as, for example, in  $\text{MgB}_2$  where intraband coupling dominates and the anisotropy doubles the transition temperature.<sup>18</sup>

Hydrogen presents a rather different situation: as the structure of the  $\bar{\lambda}$  matrix shows, interband coupling constants are very large for the most coupled regions ( $R_1$  and  $R_2$ ) and small on the less coupled ones ( $R_3$ ). Then, the main source of the multigap superconductivity is anisotropy within *off-diagonal* terms of the kernel. However, this kind of anisotropy does not lead to a sensible enhancement of the critical temperature. In fact, the dominant effect of the interband scattering processes is to destroy the effect of band anisotropy so that multigap superconductivity results in this case in a relatively modest enhancement of  $T_c$  (about 10%).

Figure 7 shows the values of the  $\Delta_{nk}$  gaps as a function of the energy from the Fermi level: applied pressure is seen to further reduce the gap anisotropy, so that at  $P=438$  GPa the three gaps can no longer be distinguished. Reduction in the band anisotropy reflects on the critical temperature, so that solution of the BCS multigap equation at higher pressure shows that anisotropy results in only 5% increase in  $T_c$  with respect to the BCS isotropic value, in substantial agreement with SCDFT calculations (Table III).

Finally, due to the stronger el-ph coupling,  $T_c$  increases from 84 K at  $P=414$  GPa to about 242 K at  $P=450$  GPa, as shown in Fig. 8 and then changes abruptly at  $P=438$  GPa

TABLE III. Superconducting gap and critical temperature in the multigap BCS approximation and SCDFT at different pressure.

$P$ (GPa)	$\frac{T_c - T_c^{iso}}{T_c} \times 100$ (BCS) (%)	$\frac{T_c - T_c^{iso}}{T_c} \times 100$ (SCDFT) (%)
414	9.4	10
438	2.9	5.6
462	2.6	4.8

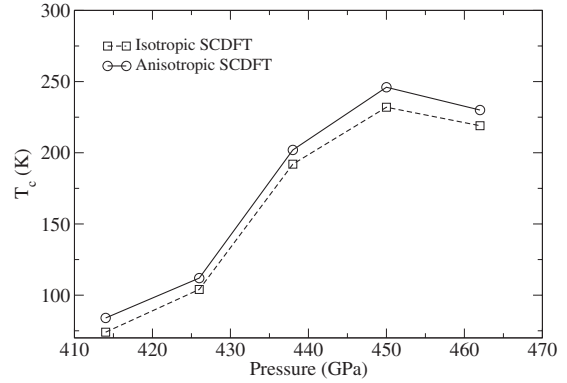


FIG. 8. Behavior of the critical temperature as a function of the pressure.

where the two additional FS sheets ( $R_4$  and  $R_5$ ) appear. Although pressure progressively reduces anisotropy (Table III) the difference between the anisotropic and isotropic  $T_c$  does not depend on pressure but is rather kept constant (about 10 K) over the entire pressure range considered, as shown in Fig. 8.

## V. CONCLUSIONS

We presented a detailed study of the electron-phonon interaction and of the mechanisms inducing high-temperature superconductivity in metallic molecular hydrogen. Analysis of the normal phase of this system revealed a very rich and complex Fermi surface characterized by many branches with different orbital character and a phonon dispersion with several softening of libron and vibron modes, arising from strong el-ph coupling. We analyzed in detail the coupling and found that it is related to two main sources: (i) intraband coupling involving libron and vibron modes at small wave vector, activating charge transfer between bonding and anti-bonding states; (ii) interband coupling mainly coming from large  $\mathbf{q}$  phononic modes and related to the complex FS structure. Due to the large number of phonon modes involved in the coupling, interband scattering processes represent the dominant contribution to  $\lambda$ . In addition, the presence of multiple Fermi surfaces provides a “ $\mathbf{q}$ -distributed” coupling, where several modes concur to the pairing: this allows to increase  $\lambda$  still avoiding a lattice instability, which could result from very large coupling at specific  $\mathbf{q}$ 's.

The very high value of the critical temperature predicted within SCDFT,  $T_c=242$  K at  $P=450$  GPa, is surprising for a phonon-mediated mechanism. This is due to large values of the phonon frequencies, related to the small proton mass, and to the presence of vibronic modes which provide a large energy window around the Fermi level for electrons to interact via phonon exchange. A large electron-phonon coupling is granted, despite the rather large values of the phonon frequencies, by two main contributions: (i) large el-ph matrix elements related to the lack of the ion-core and to the presence of strongly coupled phonon modes (libron and vibron); (ii) the mentioned  $\mathbf{q}$ -distributed coupling.

Although our computational approach can be viewed as state of the art in predicting the superconducting critical tem-

perature, our results may suffer of some approximations (as yet unavoidable). We therefore address some points that, in our opinion, are relevant in the discussion of the results presented: (i) we found that the explicit treatment of electron screening is a fundamental requirement, at least in this system. In fact, the use of a single parameter ( $\mu^*$ ), the “effective” Coulomb pseudopotential, is unjustified<sup>19</sup> since it varies from 0.16 at 414 to 0.08 at 462 GPa, due to smaller Coulomb matrix elements with increased metallization. In addition, many-body perturbation theory beyond RPA for the electron-electron interaction can produce an additional effective attractive interaction in multiband systems such as hydrogen.<sup>20,21</sup> Although not included in the present results, this contribution can be cast within our functionals and it is likely to enhance the critical temperature even further; (ii) at the insulator-metal transition, the electron and hole pockets at the Fermi surface have a rather small Fermi energy (0.2–0.3 eV). In view of the very large phonon frequencies involved, nonadiabatic effects and vertex corrections beyond Migdal approximation can be expected,<sup>22</sup> as well as possible

phonons renormalization due to nonadiabatic effects (the phonon self-energy depends on the phonon frequency). However, the inclusion of such contributions into an *ab initio* theory is not available at the moment and is not so obvious to infer its possible effect on  $T_c$ .

In conclusion, our exhaustive investigation of the *Cmca* phase of hydrogen under pressure allows a better understanding of the different mechanisms entering the superconducting properties of this system and how each of them is affected by pressure. The hope is to give insights on possible new molecular metallic systems based on light elements that might exhibit similar superconducting properties.<sup>23</sup>

#### ACKNOWLEDGMENTS

We acknowledge support from INFM-CNR through Iniziattiva di Calcolo Parallelo. Work partially supported by the Italian Ministry of Education, through PRIN 2008XWLWF9\_003 project and supercomputing grant at Cineca (Bologna, Italy).

- 
- <sup>1</sup>A. Y. Liu, I. I. Mazin, and J. Kortus, *Phys. Rev. Lett.* **87**, 087005 (2001).
- <sup>2</sup>R. S. Gonnelli, D. Daghero, D. Delaude, M. Tortello, G. A. Ummarino, V. A. Stepanov, J. S. Kim, R. K. Kremer, A. Sanna, G. Profeta, and S. Massidda, *Phys. Rev. Lett.* **100**, 207004 (2008).
- <sup>3</sup>F. Weber, A. Kreyssig, L. Pintschovius, R. Heid, W. Reichardt, D. Reznik, O. Stockert, and K. Hradil, *Phys. Rev. Lett.* **101**, 237002 (2008).
- <sup>4</sup>Y. Nakajima, T. Nakagawa, T. Tamegai, and H. Harima, *Phys. Rev. Lett.* **100**, 157001 (2008).
- <sup>5</sup>C. L. Huang, J.-Y. Lin, Y. T. Chang, C. P. Sun, H. Y. Shen, C. C. Chou, H. Berger, T. K. Lee, and H. D. Yang, *Phys. Rev. B* **76**, 212504 (2007).
- <sup>6</sup>R. S. Gonnelli, D. Daghero, M. Tortello, G. A. Ummarino, V. A. Stepanov, R. K. Kremer, J. S. Kim, N. D. Zhigadlo, and J. Karpinski, *Physica C* **469**, 512 (2009).
- <sup>7</sup>P. Szabó, Z. Pribulova, G. Pristas, S. L. Bud'ko, P. C. Canfield, and P. Samuely, *Phys. Rev. B* **79**, 012503 (2009).
- <sup>8</sup>C. Ren, W. Zhao-sheng, L. Hui-qian, H. Yang, L. Shan, and H.-H. Wen, *Phys. Rev. Lett.* **101**, 257006 (2008).
- <sup>9</sup>P. Cudazzo, G. Profeta, A. Sanna, A. Floris, A. Continenza, S. Massidda, and E. K. U. Gross, *Phys. Rev. Lett.* **100**, 257001 (2008).
- <sup>10</sup>L. N. Oliveira, E. K. U. Gross, and W. Kohn, *Phys. Rev. Lett.* **60**, 2430 (1988).
- <sup>11</sup>M. Lüders, M. A. L. Marques, N. N. Lathiotakis, A. Floris, G. Profeta, L. Fast, A. Continenza, S. Massidda, and E. K. U. Gross, *Phys. Rev. B* **72**, 024545 (2005).
- <sup>12</sup>M. A. L. Marques, M. Lüders, N. N. Lathiotakis, G. Profeta, A. Floris, L. Fast, A. Continenza, E. K. U. Gross, and S. Massidda, *Phys. Rev. B* **72**, 024546 (2005).
- <sup>13</sup>P. Cudazzo, G. Profeta, A. Sanna, A. Floris, A. Continenza, S. Massidda, and E. K. U. Gross, *Phys. Rev. B* **81**, 134505 (2010).
- <sup>14</sup>L. Zhang, Y. Niua, Q. Lia, T. Cuia, Y. Wanga, Y. Ma, Z. Hea, and G. Zoua, *Solid State Commun.* **141**, 610 (2007).
- <sup>15</sup>P. Cudazzo, Ph.D. thesis, University of L'Aquila, 2008.
- <sup>16</sup>F. S. Khan and P. B. Allen, *Phys. Rev. B* **29**, 3341 (1984).
- <sup>17</sup>L. J. Sham and W. Kohn, *Phys. Rev.* **145**, 561 (1966).
- <sup>18</sup>A. Floris, G. Profeta, N. N. Lathiotakis, M. Lüders, M. A. L. Marques, C. Franchini, E. K. U. Gross, A. Continenza, and S. Massidda, *Phys. Rev. Lett.* **94**, 037004 (2005).
- <sup>19</sup>C. F. Richardson and N. W. Ashcroft, *Phys. Rev. Lett.* **78**, 118 (1997).
- <sup>20</sup>C. F. Richardson and N. W. Ashcroft, *Phys. Rev. B* **55**, 15130 (1997).
- <sup>21</sup>G. Vignale and K. S. Singwi, *Phys. Rev. B* **31**, 2729 (1985).
- <sup>22</sup>E. Cappelluti, S. Ciuchi, C. Grimaldi, L. Pietronero, and S. Strässler, *Phys. Rev. Lett.* **88**, 117003 (2002).
- <sup>23</sup>M. I. Eremets, I. A. Trojan, S. A. Medvedev, J. S. Tse, and Y. Yao, *Science* **319**, 1506 (2008).